Rossby Wave Frequencies and Group Velocities for Finite Element and Finite Difference Approximations to the Vorticity-Divergence and the Primitive Forms of the Shallow Water Equations

BENY NETA AND R. T. WILLIAMS

Naval Postgraduate School, Monterey, California

(Manuscript received 16 August 1988, in final form 23 January 1989)

ABSTRACT

In this paper Rossby wave frequencies and group velocities are analyzed for various finite element and finite difference approximations to the vorticity-divergence form of the shallow water equations. Also included are finite difference solutions for the primitive equations for the staggered grids B and C from Wajsowicz and for the unstaggered grid A. The results are presented for three ratios between the grid size and the Rossby radius of deformation. The vorticity-divergence equation schemes give superior solutions to those based on the primitive equations. The best results come from the finite element schemes that use linear basis functions on isosceles triangles and bilinear functions on rectangles. All of the primitive equation finite difference schemes have problems for at least one Rossby deformation-grid size ratio.

1. Introduction

The hydrostatic primitive equation numerical models that are used for atmospheric and oceanographic prediction permit inertial gravity waves, Rossby waves, and advective effects. The influence of a numerical scheme on each of these types of motion is most easily analyzed by separating the linearized prediction equations into vertical modes with an equivalent depth analysis (for example, see Gill 1982). In this case the equations for each vertical mode are just the linearized shallow equations with the appropriate equivalent depth. In fact, one must also consider the vertical differencing in deriving the shallow water system, but we will not treat these effects in this paper. Arakawa and Lamb (1977) analyzed inertial gravity wave motions for four finite difference grids that they labeled A, B, C, and D. They found that the geostrophic adjustment for the unstaggered grid A and grid D is poor and that the adjustment for grids B and C is good. Schoenstadt (1980) studied geostrophic adjustment for finite elements with piecewise linear basis functions with the nodal points located at the finite difference grid points. He determined that the unstaggered finite element scheme (grid A) gives poor adjustment for small scale motions, but the schemes B and C are excellent. Williams (1981) examined geostrophic adjustment in the vorticity-divergence form of the shallow water equations with finite difference and finite element schemes. He showed that the nonstaggered vorticity-divergence schemes give as good geostrophic adjustment as the best staggered shallow water schemes. Since finite element models with staggered basis functions are much more complicated, especially in two dimensions, the best finite element schemes for geostrophic adjustment use the vorticity-divergence formulation. Some examples of atmospheric prediction models of this type are given by Staniforth and Mitchell (1977, 1978), Staniforth and Daley (1979), and Cullen and Hall (1979).

The objective of this study is to investigate the treatment of Rossby waves in vorticity-divergence shallow water formulations with various finite element and finite difference schemes. For comparison the finite difference primitive equation solutions for grids A, B, and C are also included. The finite difference solutions for grids B and C are taken from a recent and very complete study by Wajsowicz (1986). An earlier, one-dimensional study on these grids was carried out by Mesinger (1979).

Corresponding author address: Dr. R. T. Williams, Department of Meteorology, Naval Postgraduate School, Monterey, CA 93943-5000.

2. Basic equations

The linearized shallow water equations on a beta plane can be written

$$\frac{\partial u}{\partial t} - fv + g\frac{\partial h}{\partial x} = 0, \tag{2.1}$$

$$\frac{\partial v}{\partial t} + fu + g\frac{\partial h}{\partial y} = 0, \tag{2.2}$$

$$\frac{\partial h}{\partial t} + gH\left(\frac{\partial u}{\partial x} + \frac{\partial v}{\partial y}\right) = 0, \qquad (2.3)$$

where u and v are the velocity perturbations, h is the height perturbation and H the equivalent depth, and f is the Coriolis parameter. The vorticity-divergence equation set, which is obtained by differentiating (2.1) and (2.2) with respect to x and y respectively and combining, can be written

$$\frac{\partial \zeta}{\partial t} + fD + v\beta = 0, \qquad (2.4)$$

$$\frac{\partial D}{\partial t} - f\zeta + u\beta + g\left(\frac{\partial^2 h}{\partial x^2} + \frac{\partial^2 h}{\partial y^2}\right) = 0, \qquad (2.5)$$

$$\frac{\partial h}{\partial t} + HD = 0, \qquad (2.6)$$

where $\beta = df/dy$,

$$\zeta = \frac{\partial v}{\partial x} - \frac{\partial u}{\partial y}$$

and

$$D = \frac{\partial u}{\partial x} + \frac{\partial v}{\partial y}.$$

To isolate the Rossby mode more easily we apply the quasi-geostrophic approximation to the set (2.4)–(2.6), (for example, see Chapter 3 in Haltiner and Williams 1980):

$$\frac{\partial \zeta}{\partial t} + f_0 D + \frac{1}{f_0} g \frac{\partial h}{\partial x} \beta_0 = 0, \qquad (2.7)$$

$$-f_0\zeta + g\left(\frac{\partial^2 h}{\partial x^2} + \frac{\partial^2 h}{\partial y^2}\right) = 0, \qquad (2.8)$$

$$\frac{\partial h}{\partial t} + HD = 0, \qquad (2.9)$$

where f_0 and β_0 are evaluated at an appropriate central latitude.

The plane wave expression for the Rossby wave frequency is obtained by inserting the wave forms

$$\begin{bmatrix} \zeta \\ D \\ h \end{bmatrix} = \begin{bmatrix} \zeta_0 \\ D_0 \\ h_0 \end{bmatrix} e^{i(\mu x + ky - \omega t)} \qquad (2.10)$$

into (2.7)–(2.9) which gives

$$\omega = \frac{-\mu\beta_0}{\mu^2 + k^2 + \lambda^{-2}}, \qquad (2.11)$$

where $\lambda = (gH)^{1/2}/f_0$ is the Rossby radius of deformation. The two components of the group velocity are given by

TABLE 1. The operators for the various numerical schemes for the shallow water equations. ($X = \mu\Delta x$, $Y = k\Delta y$).

Scheme		Vorticity-divergence form: Finite element		Vorticity-divergence form: Finite differences		Primitive equation form: Finite difference		
Operator	Analytic	Isosceles triangles	Rectangular	Second-order	Fourth-order	A	B	C
α	1	$(3 + \cos X + 2\cdot\cos X/2\cos Y)/6$	$(2 + \cos X)\cdot(2 + \cos Y)/9$	1	1	1	1	$\cos^2(X/2)\cos^2(Y/2)$
θ	μ	$2(\sin X + \sin(X/2)\cdot\cos Y)/(3\Delta x)$	$\sin X(2 + \cos Y)/(3\Delta x)$	$\frac{\sin X}{\Delta x}$	$\frac{4}{3}\frac{\sin X}{\Delta x} - \frac{1}{6}\frac{\sin(2X)}{\Delta x}$	$\frac{\sin X}{\Delta x}\cos(Y/2)$	$\frac{\sin X}{\Delta x}$	$\frac{\sin X}{\Delta x}\cos^2(Y/2)$
δ	μ^2	$\frac{\sin^2(X/2)}{(\Delta x/2)^2}$	$\frac{\sin^2(X/2)}{(\Delta x/2)^2}\cdot(2 + \cos Y)/3$	$\frac{\sin^2(X/2)}{(\Delta x/2)^2}$	$\frac{\cos(2X) - 16\cos X + 15}{6\Delta x^2}$	$\frac{\sin^2 X}{\Delta x^2}$	$\frac{\sin^2(X/2)}{(\Delta x/2)^2}\frac{1 + \cos Y}{2}$	$\frac{\sin^2(X/2)}{(\Delta x/2)^2}$
ϵ	k^2	$\frac{(3 + \cos X - 4\cos(X/2)\cdot\cos Y)/}{(2\Delta y^2)}$	$\frac{\sin^2(Y/2)}{(\Delta y/2)^2}\cdot(2 + \cos X)/3$	$\frac{\sin^2(Y/2)}{(\Delta y/2)^2}$	$\frac{\cos(2Y) - 16\cos Y + 15}{6\Delta y^2}$	$\frac{\sin^2 Y}{\Delta y^2}$	$\frac{\sin^2(Y/2)}{(\Delta y/2)^2}\frac{1 + \cos X}{2}$	$\frac{\sin^2(Y/2)}{(\Delta y/2)^2}$

TABLE 2. The derivatives required for the group velocity.

Scheme		Vorticity-divergence form				Primitive equation form		
		Finite element		Finite difference				
Deriv-ative	Ana-lytic	Isosceles triangles	Rectangles	Second-order	Fourth-order	Scheme A	Scheme B	Scheme C
$\frac{\partial\alpha}{\partial\mu}$	0	$-\Delta x(\sin X + \sin(X/2)\cos Y)/6$	$-\Delta x(2+\cos Y)\cdot(\sin X)/9$	0	0	0	0	$-\Delta x \sin X\cdot\cos^2(Y/2)/2$
$\frac{\partial\theta}{\partial\mu}$	1	$2\left(\cos X + \frac{1}{2}\cdot\cos(X/2)\cos Y\right)\Big/3$	$\cos X(2+\cos Y)/3$	$\cos X$	$\frac{4}{3}\cos X - \frac{1}{3}\cos 2x$	$\cos X\cos Y$	$\cos X$	$\cos X\cos^2(Y/2)$
$\frac{\partial\delta}{\partial\mu}$	2μ	$2\sin X/\Delta x$	$2\sin X\cdot(2+\cos Y)/(3\Delta x)$	$\frac{2\sin X}{\Delta x}$	$\frac{8\sin X - \sin 2X}{3\Delta x}$	$\frac{\sin 2X}{\Delta x}$	$\frac{\sin X}{\Delta x}(1+\cos Y)$	$\frac{2\sin X}{\Delta x}$
$\frac{\partial\epsilon}{\partial\mu}$	0	$-\Delta x(\sin X - 2\cdot\sin(X/2)\cos Y)/(2\Delta y^2)$	$-\Delta x\sin X\cdot\sin^2(Y/2)/3(\Delta y/2)^2$	0	0	0	$-\frac{\Delta x}{2(\Delta y/2)^2}\sin X\cdot\sin^2(Y/2)$	0
$\frac{\partial\alpha}{\partial k}$	0	$-\Delta y\cos(X/2)\cdot\sin Y/3$	$-\Delta y(2+\cos X)\cdot(\sin Y)/9$	0	0	0	0	$-\Delta y\cos^2(X/2)\sin(Y/2)$
$\frac{\partial\theta}{\partial k}$	0	$-\frac{2}{3}\frac{\Delta y}{\Delta x}\sin(X/2)\cdot\sin Y$	$-\frac{1}{3}\frac{\Delta y}{\Delta x}\sin X\sin Y$	0	0	$-\frac{\Delta y}{\Delta x}\sin X\sin Y$	0	$-\frac{\Delta y}{2\Delta x}\sin X\sin Y$
$\frac{\partial\delta}{\partial k}$	0	0	$-\frac{1}{3}\frac{\Delta y}{(\Delta x/2)^2}\sin^2(X/2)\sin Y$	0	0	0	$\frac{-\Delta y}{2(\Delta x/2)^2}\sin^2(X/2)\sin Y$	0
$\frac{\partial\epsilon}{\partial\kappa}$	$2k$	$-\frac{2}{\Delta y}\cos(X/2)\sin Y$	$\frac{2}{3\Delta y}\sin Y\cdot(2+\cos X)$	$2\frac{\sin Y}{\Delta y}$	$\frac{8\sin Y - \sin 2Y}{3\Delta y}$	$\frac{\sin 2Y}{\Delta y}$	$\frac{\sin Y}{\Delta y}(1+\cos X)$	$\frac{2\sin Y}{\Delta y}$

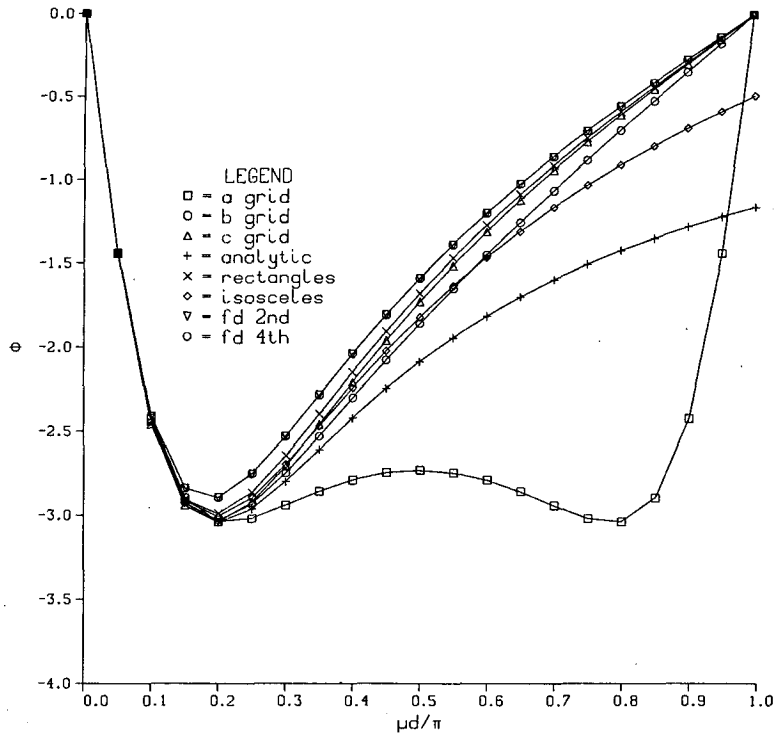

FIG. 1. The frequency ω_F, for $k = 0$ and $r^2 = 0.1$ as a function of $\mu d/\pi$ for the various schemes for each value of r^2, ω, G^x and G^y are scaled to be of order one.

$$G^x = \frac{\partial \omega}{\partial \mu} = \beta_0 \frac{[\mu^2 - (k^2 + \lambda^{-2})]}{(\mu^2 + k^2 + \lambda^{-2})^2}, \quad (2.12)$$

and

$$G^y = \frac{\partial \omega}{\partial k} = \frac{2\beta_0 \mu k}{(\mu^2 + k^2 + \lambda^{-2})^2}. \quad (2.13)$$

3. Solutions for numerical schemes

Neta and Williams (1986) analyzed the linear advection equation for various finite element schemes with linear basis functions on triangular elements and one scheme with bilinear basis functions on rectangles. They also included second- and fourth-order finite differences in the study. They found that the best schemes used the linear elements on isosceles triangles and bilinear elements on rectangles. In the current study for the vorticity-divergence formulation we will restrict ourselves to these two finite element schemes and second- and fourth-order finite difference schemes. Each of these schemes treats each grid point or nodal point in the same way so that we can follow the procedure used by Cote et al. (1983) and Neta et al. (1986). After the equations (2.7)–(2.9) have been discretized in x and y, we introduce the wave form $\exp[i(\mu x + ky)]$ that leads to

$$\alpha \frac{\partial \zeta}{\partial t} + f_0 \alpha D + \frac{\beta_0}{f_0} i\theta g h = 0. \quad (3.1)$$

$$-f_0 \alpha \zeta - g(\delta + \epsilon)h = 0, \quad (3.2)$$

$$H\alpha D + \alpha \frac{\partial h}{\partial t} = 0, \quad (3.3)$$

where α, θ, δ, and ϵ depend on the scheme. These new parameters are given in Table 1 for the two finite element and the two finite difference schemes for vorticity-divergence form of the equations. The procedure for obtaining the parameters is given in appendix A.

The frequency can now be obtained by introducing the dependence $\exp[-i\omega_F t]$ into the set (3.1)–(3.3) giving

$$\omega_F = \frac{-\beta_0 \theta}{\delta + \epsilon + \alpha\lambda^{-2}}, \quad (3.4)$$

where ω_F is the frequency for the numerical scheme with continuous time variation.

Wajsowicz (1986) has derived expressions for ω_F from the primitive form of the shallow water equations for staggered grids B and C. For completeness we derive the expression for unstaggered grid A in appendix B. In each case, the frequency can be written in the form (3.4) with the corresponding parameters given in Table 1.

The group velocities for the numerical schemes can be obtained by differentiating (3.4) as follows:

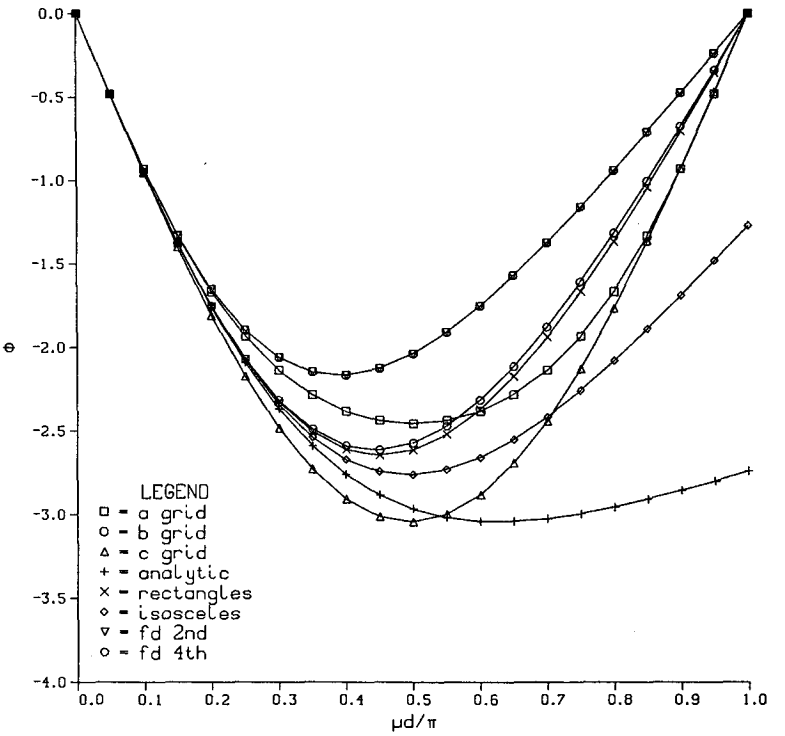

FIG. 2. Same as Fig. 1 except that $r^2 = 1$.

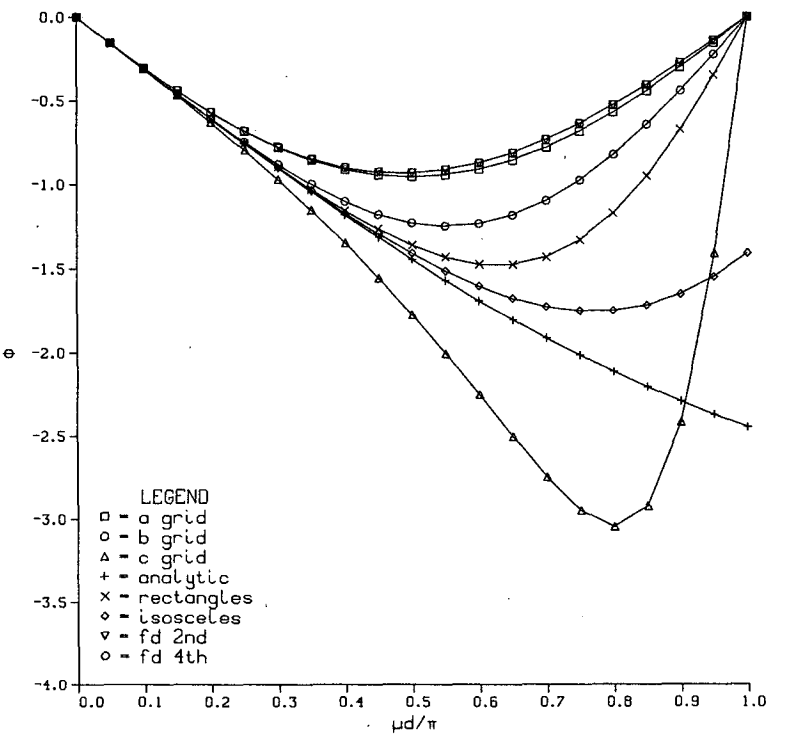

FIG. 3. Same as Fig. 1 except that $r^2 = 10$.

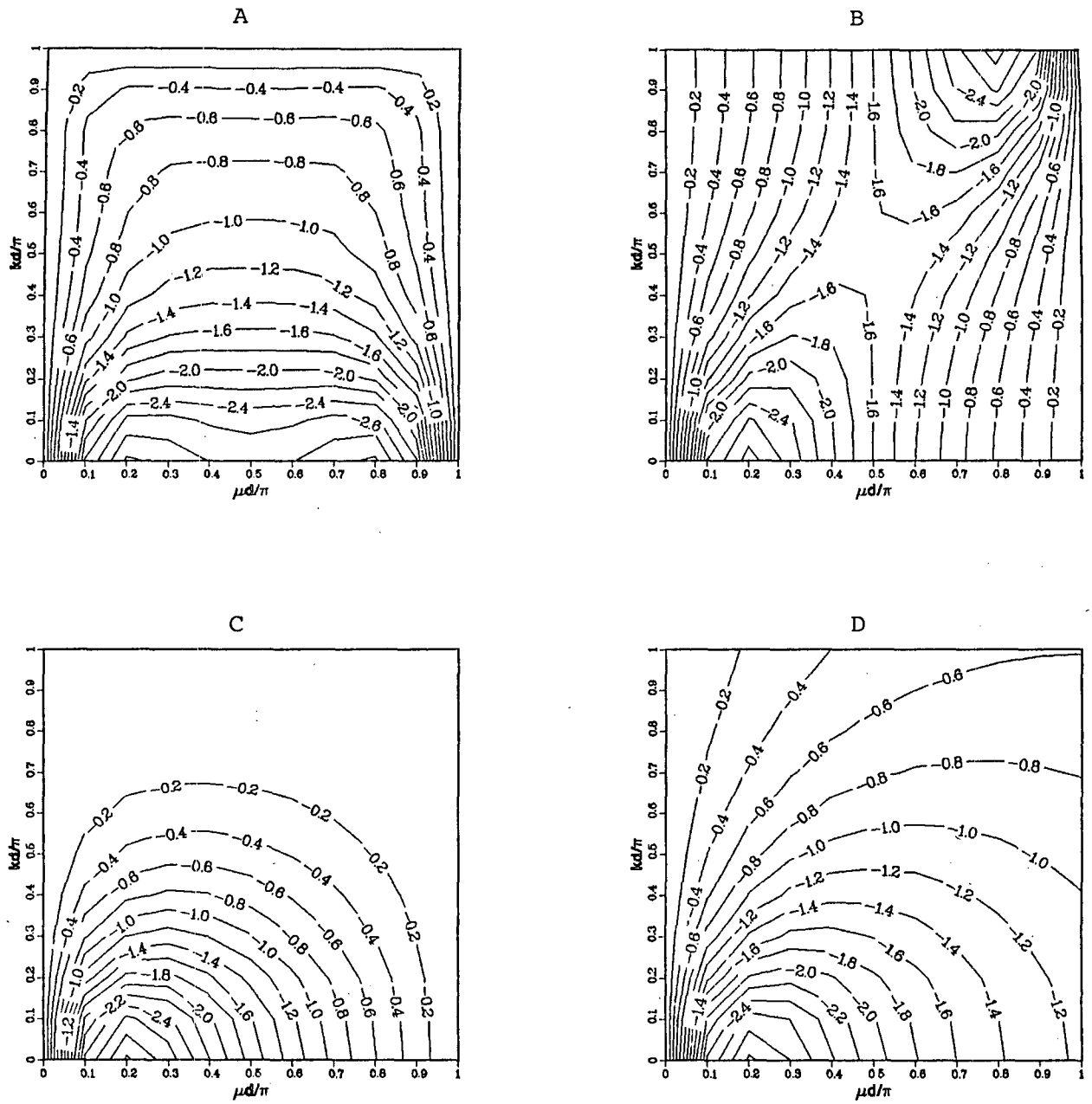

FIG. 4. The frequency ω_F, as a function of $\mu d/\pi$ and kd/π for $r^2 = 0.1$. The following figure labels correspond to the following schemes: (a) finite difference scheme A, primitive equations formulation; (b) finite difference scheme B, primitive equation formulation; (c) finite difference scheme C, primitive equation formulation; (d) analytic solution; (e) second-order finite difference, vorticity-divergence formulation; (f) fourth-order finite difference, vorticity-divergence formulation; (g) bilinear finite elements on rectangles, vorticity-divergence formulations; (h) linear finite elements on isosceles triangles, vorticity-divergence formulation.

$$G_F{}^x = \frac{\partial \omega_F}{\partial \mu} = -\beta_0 \times \frac{\dfrac{\partial \theta}{\partial \mu}[\delta + \epsilon + \alpha\lambda^{-2}] - \theta\left[\dfrac{\partial \delta}{\partial \mu} + \dfrac{\partial \epsilon}{\partial \mu} + \lambda^{-2}\dfrac{\partial \alpha}{\partial \mu}\right]}{[\delta + \epsilon + \alpha\lambda^{-2}]^2}, \tag{3.5}$$

$$G_F{}^y = \frac{\partial \omega_F}{\partial k} = -\beta_0 \times \frac{\dfrac{\partial \theta}{\partial k}[\delta + \epsilon + \alpha\lambda^{-2}] - \theta\left[\dfrac{\partial \delta}{\partial k} + \dfrac{\partial \epsilon}{\partial k} + \lambda^{-2}\dfrac{\partial \alpha}{\partial k}\right]}{[\delta + \epsilon + \alpha\lambda^{-2}]^2}. \tag{3.6}$$

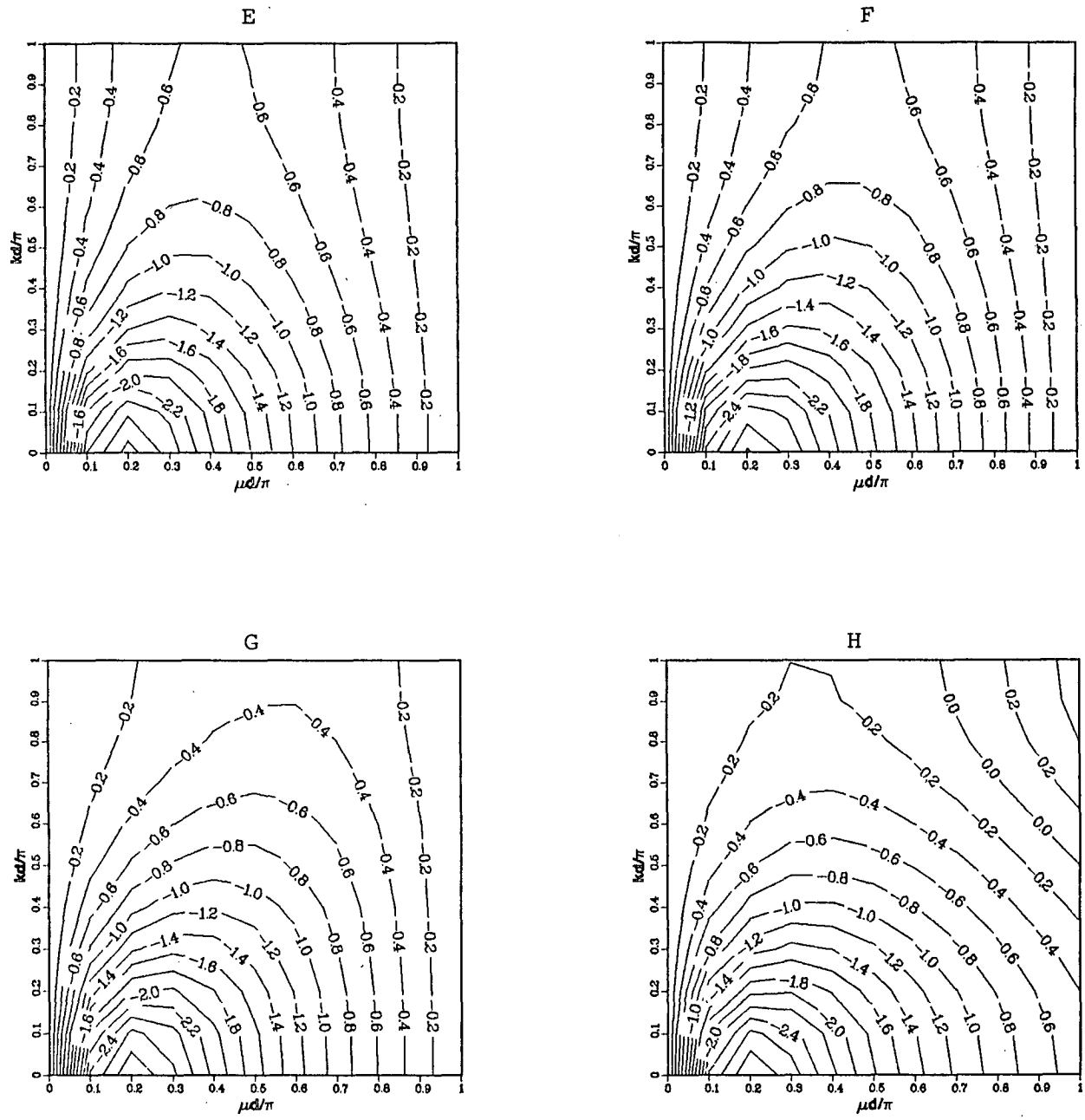

FIG. 4. (*Continued*)

The required derivatives for (3.5) and (3.6) are given for the vorticity-divergence schemes and the primitive equation schemes in Table 2.

4. Results

In this section the frequencies and group velocities for the various numerical schemes will be represented and discussed. Following Wajsowicz (1986), results will be given for $r^2 = d^2/(4\lambda^2) = 0.1$, 1.0 and 10. Also, we set $d = \Delta x = \Delta y$. The parameter r^2 measures the relative importance of the terms in the denominator of (3.4) when the wave scale is small. In order to more easily compare the schemes, we will first examine the frequency for $k = 0$ as a function of $\mu d/\pi$. Figure 1 gives the frequency for each scheme for $d^2/(4\lambda^2) = 0.1$. The analytic formula for the frequency (2.11), shows that for $k = 0$, ω goes to zero as either $\mu \to 0$ or $\mu \to \infty$ and it has a minimum at $\mu = \lambda^{-1}$. All of the schemes handle the behavior as $\mu \to 0$ very well because

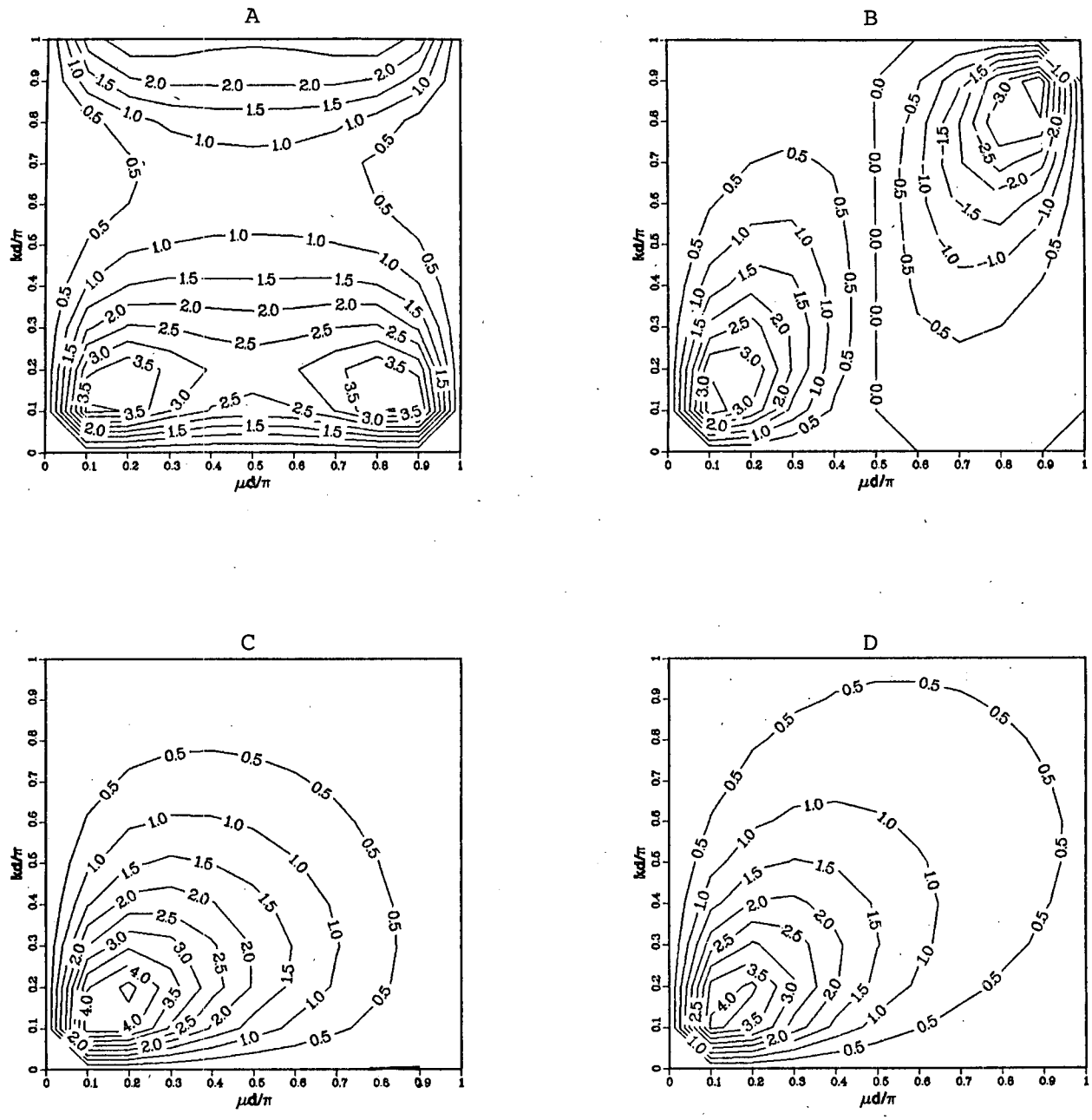

FIG. 5. The eastward component of group velocity G_F^x as a function of $\mu d/\pi$ and kd/π for $r^2 = 0.1$, with scheme labels as in Fig. 4.

the wave resolution is exact in this limit. For $\mu > \pi/2d$, however, the curves depart from the exact solution and, in some cases, from each other. All of the schemes except the FEM scheme with isosceles triangles go to zero at the minimum scale where $\mu = \pi/d$. This behavior can be explained by examining θ which approximates the x-wavenumber μ as defined in Table 1. All of the schemes that go to zero calculate $\partial h/\partial x$ in the beta term over two grid lengths since they are represented by $(\sin\mu d)/d$ which is zero for $\mu d = \pi$. The isosceles triangle FEM scheme provides a more accurate representation for $\partial h/\partial x$ since it also involves points $(x \pm d/2, y \pm d/2)$ in the formula (see Neta and Williams 1986). All of the other schemes, except our FD scheme A, are very similar, and they underestimate the magnitude of the frequency. The poor behavior of FD scheme A can be traced to the poor representation of μ^2 by δ in Table 1. This is especially critical in this case where λ^{-2} is small as can be seen from (3.4). Also note that the group velocity for scheme

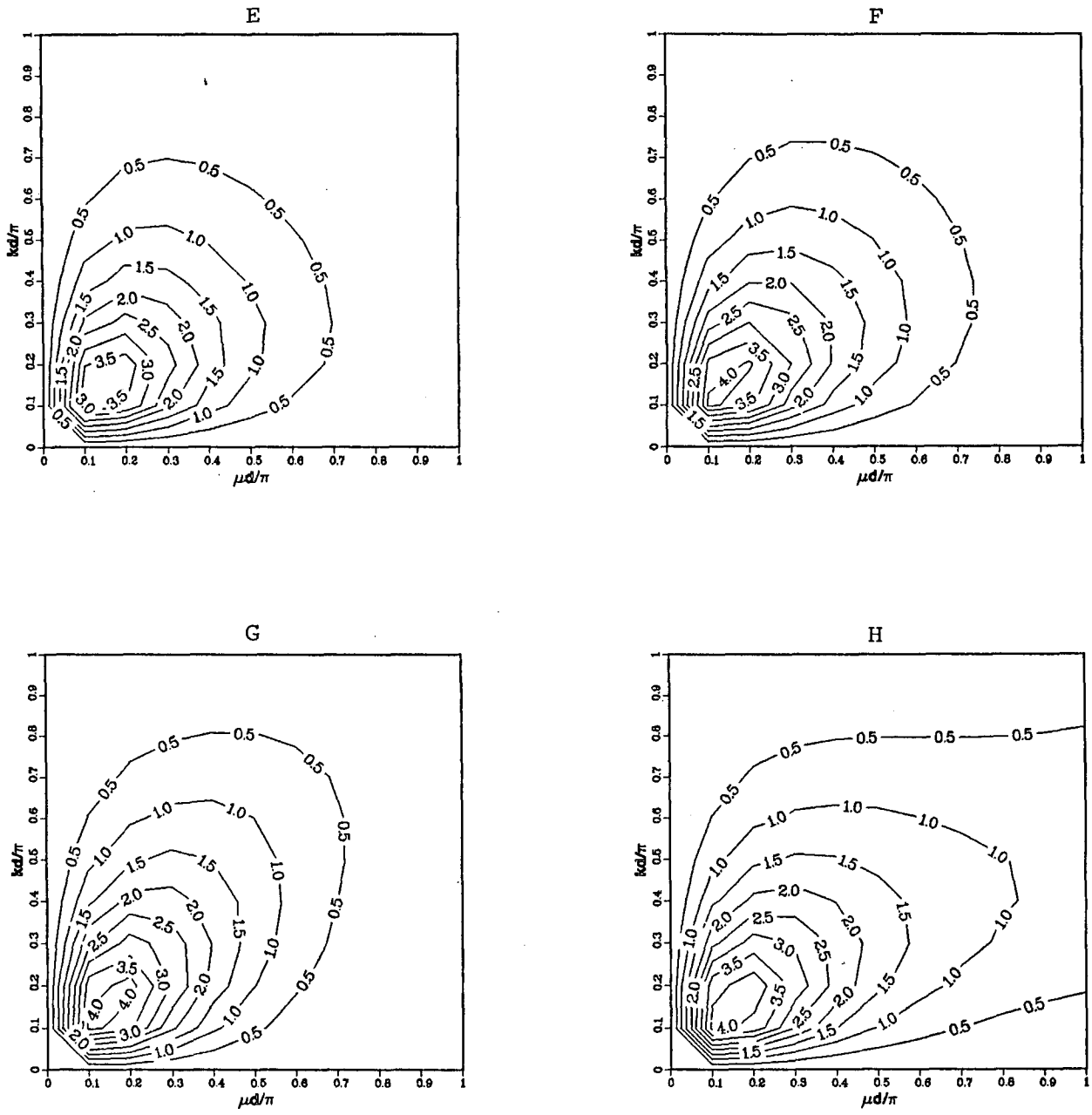

FIG. 5. (*Continued*)

A is excessively large for short wavelengths because of the steep slope of the frequency curve.

The frequency curves for $k = 0$ and $d^2/(4\lambda^2) = 1.0$ are given in Fig. 2. The general behavior is similar to Fig. 1 with certain exceptions. All schemes have larger errors as $\mu d/\pi$ approaches 1 because the analytic solution is near its maximum value there, and the isosceles FEM scheme is the best in this area since it does not drop all the way to zero. Near $\mu d/\pi = \frac{1}{2}$, FD scheme C gives the best results, but it then drops off to zero. The poorest schemes are FD scheme B and the second-order vorticity-divergence FD scheme. These schemes are equivalent whenever $k = 0$. The FD scheme A does not give poor results in this case because the λ^{-2} term in the denominator of (3.4) is not small, so that the underestimate of δ is not so important.

The frequency curves for $k = 0$ and $d^2/(4\lambda^2) = 10$ are given in Fig. 3. In this case the analytic solution is still decreasing at $\mu d/\pi = 1$. The isosceles triangle FEM

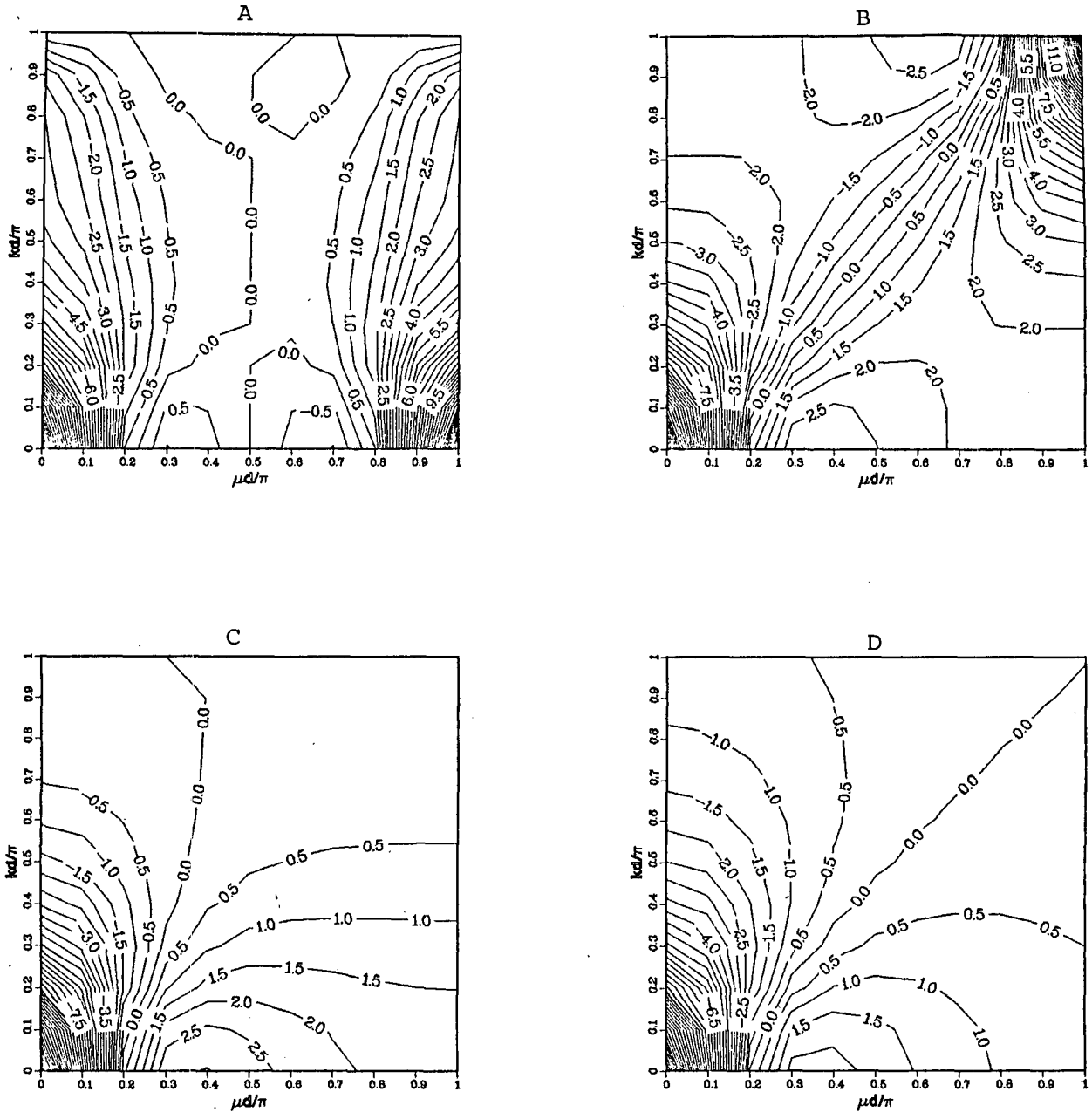

FIG. 6. The northward component of group velocity G_F^y as a function of $\mu d/\pi$ and kd/π for $r^2 = 0.1$, with scheme labels as in Fig. 4.

scheme is again the best. The FD scheme C considerably overshoots the analytic solution before it drops to zero at $\mu d/\pi = 1$ which also occurs in Fig. 2 to a lesser extent. This behavior is caused by the averaging that is required in scheme C represented by α in Table 1. This is crucial in this case because the λ^{-2} is the dominant term in the denominator of (3.4). Note that scheme C has excessive group velocity of the wrong sign near $\mu d/\pi = 1$. These three cases with $k = 0$ all show that the isosceles triangles FEM scheme in the vorticity-divergence form gives the best results and the FEM scheme with bilinear basis functions on rectangles the second best. All of the FD schemes (A, B, and C) for the primitive equations give poor results in at least one case.

With this background for the $k = 0$, we will now examine the frequency and group velocity components as functions of μ and k for each scheme. The quantities

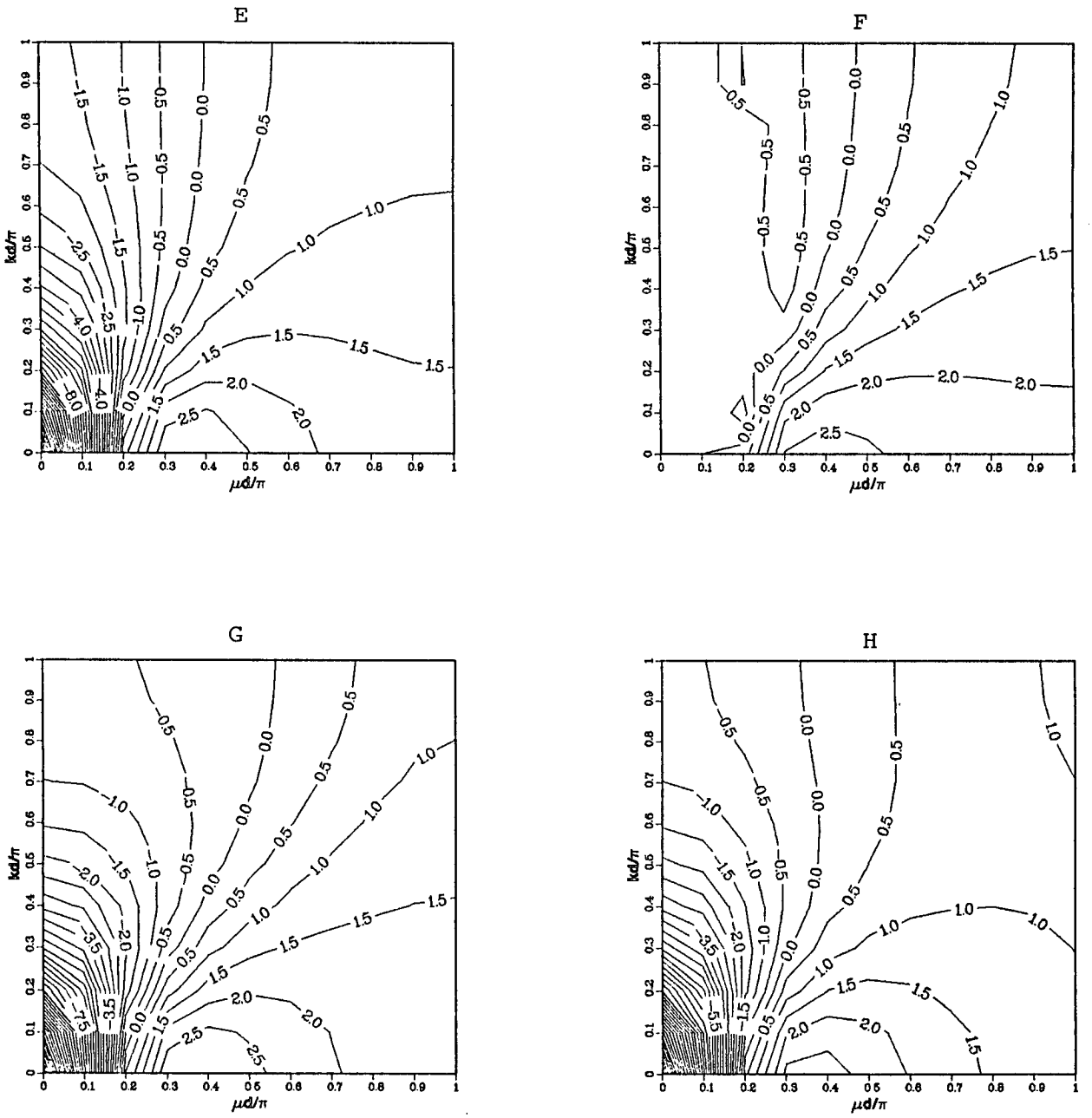

FIG. 6. (*Continued*)

ω_F, $G_F{}^x$, and $G_F{}^y$ are computed from (3.4), (3.5), and (3.6) respectively, with the relations given in Tables 1 and 2. Figures 4, 5, and 6 contain ω_F, $G_F{}^x$, and $G_F{}^y$ for the case $d^2/(4\lambda^2) = 0.1$. The analytic solution for ω is given in Fig. 4d. For this case, FD scheme C (Fig. 4c) is clearly better than FD schemes A (Fig. 4a) and B (Fig. 4b) when compared with the analytic solution. In particular, Fig. 4a shows a rapid change in ω_F for scheme A near ($\mu d/\pi = 1.0$, $k = 0$) leading to excessive values of $G_F{}^x$ and $G_F{}^y$ as can be seen when Figs. 5a and 6a are compared with Figs. 5d and 6d. A similar problem occurs for scheme B near ($\mu d/\pi = 1.0$, $kd/\pi = 1.0$) (Fig. 4b) which is associated with spuriously large values of $G_F{}^x$ and $G_F{}^y$ in Figs. 5b and 6b. The following schemes that are based on the vorticity-divergence form of the equations: second-order FD (Fig. 4e), fourth-order FD (Fig. 4f) and FEM on rectangles (Fig. 4g), are very similar, and they compare well with

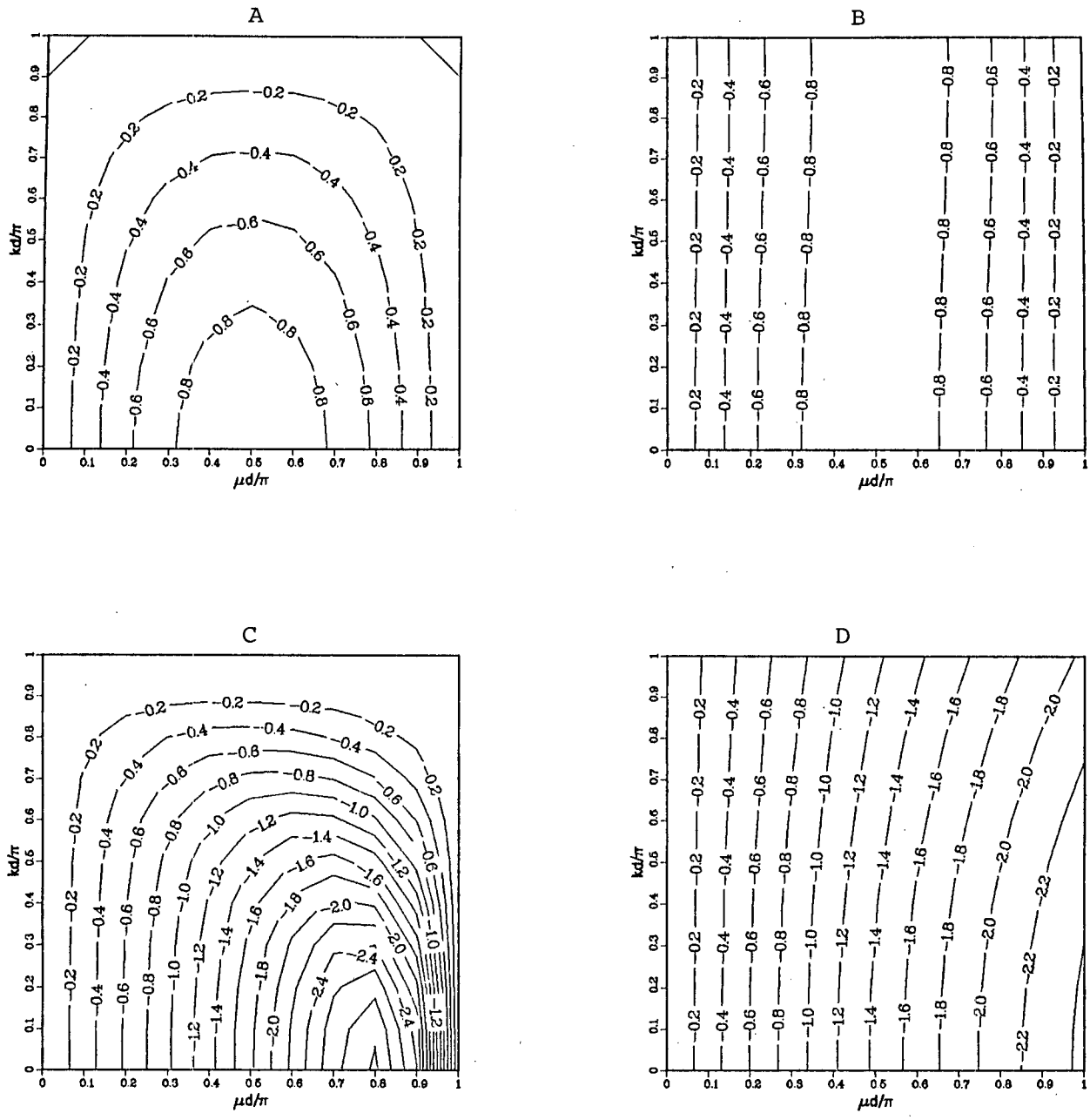

FIG. 7. Same as Fig. 4 except that $r^2 = 10$.

the exact solution (Fig. 4d). The FEM scheme is the best of these three, and the second-order FD is the poorest. The isosceles FEM (Fig. 4h) has a generally similar behavior, but it is better for small k and a little poorer near the corner ($\mu d/\pi = 1.0, kd/\pi = 1.0$). The μ–k plots for $d^2/(4\lambda^2) = 1.0$ will not be given because the results given in Fig. 2 are quite representative.

The frequency ω_F and the group velocities $G_F{}^x$ and $G_F{}^y$ are given in Figs. 7, 8, and 9 respectively, for $d^2/(4\lambda^2) = 10$. The FD scheme C (Fig. 7c) has very large gradients in ω_F near ($\mu d/\pi = 1, k = 0$), and the wrong behavior above the diagonal from this corner. Figure 8 shows that the x-group velocity has the wrong sign and is an order of magnitude too large. A check of the other schemes in Fig. 8 shows that they all give the wrong group velocity direction in this region, but the speeds are an order of magnitude less than for FD scheme C. Figure 9 indicates that $G_F{}^y$ for scheme C is

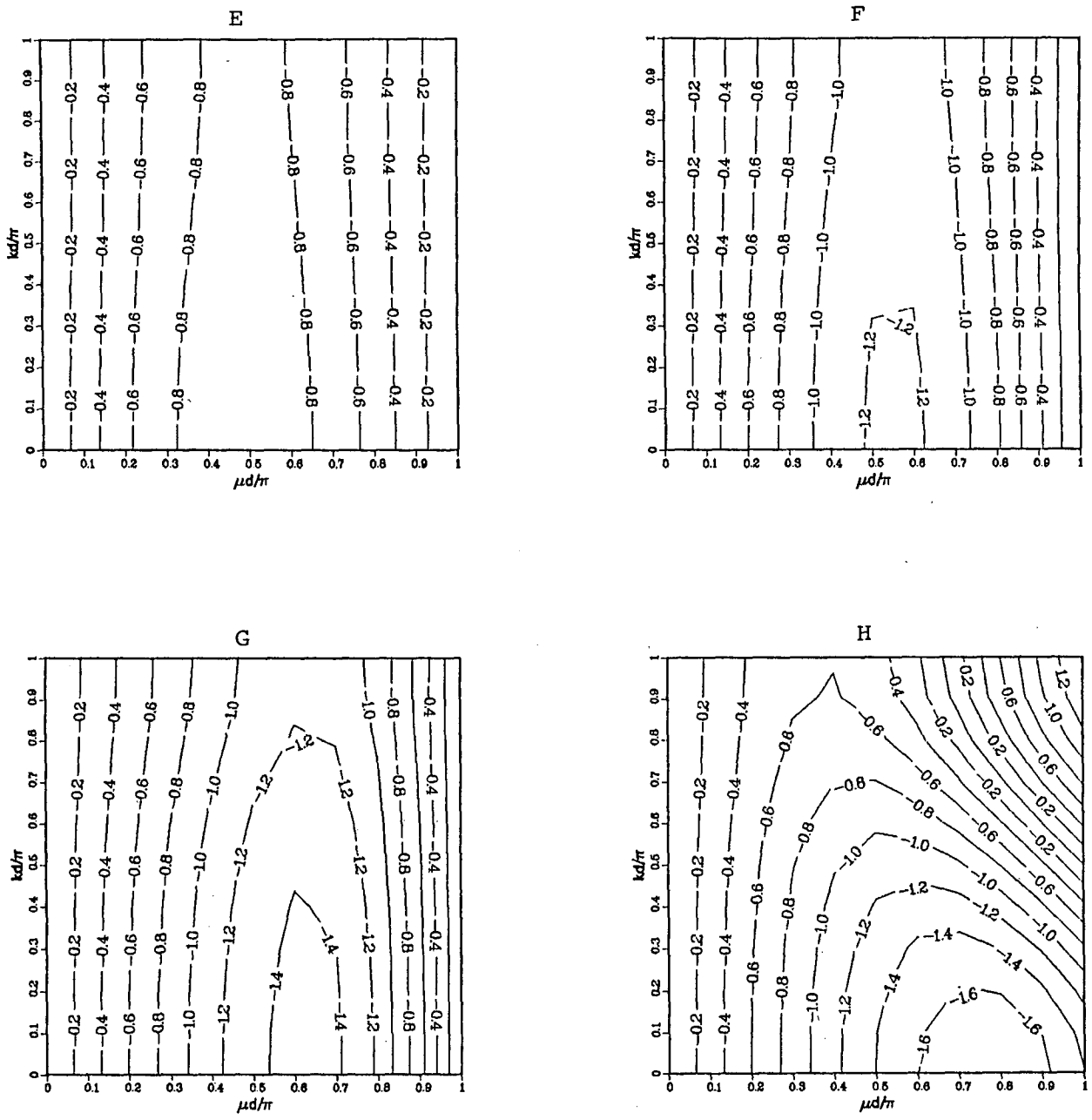

FIG. 7. (*Continued*)

also an order of magnitude too large above the diagonal. The FD schemes A (Fig. 9a) and B (Fig. 9b) do not have poor behavior, and the other schemes are similar in pattern to the other cases. The exception is the isosceles triangle FEM scheme (Fig. 9h) which gives a spurious positive frequency near $\mu d/\pi = 1$. This leads to excessively large values of G_F. The behavior in this region is related to the expression for $\partial h/\partial x$ on the isosceles triangles that leads to a poor representation for small y-scales (see Neta and Williams 1986).

5. Conclusions

In this paper we analyze Rossby wave frequencies and group velocities for various finite element and finite difference approximations to the vorticity-divergence form of the shallow water equations. Also included are finite difference solutions for the primitive equations for grids A, B, and C. The results for the staggered grids B and C are taken from Wajsowicz (1986). The equations are evaluated in three categories where the grid

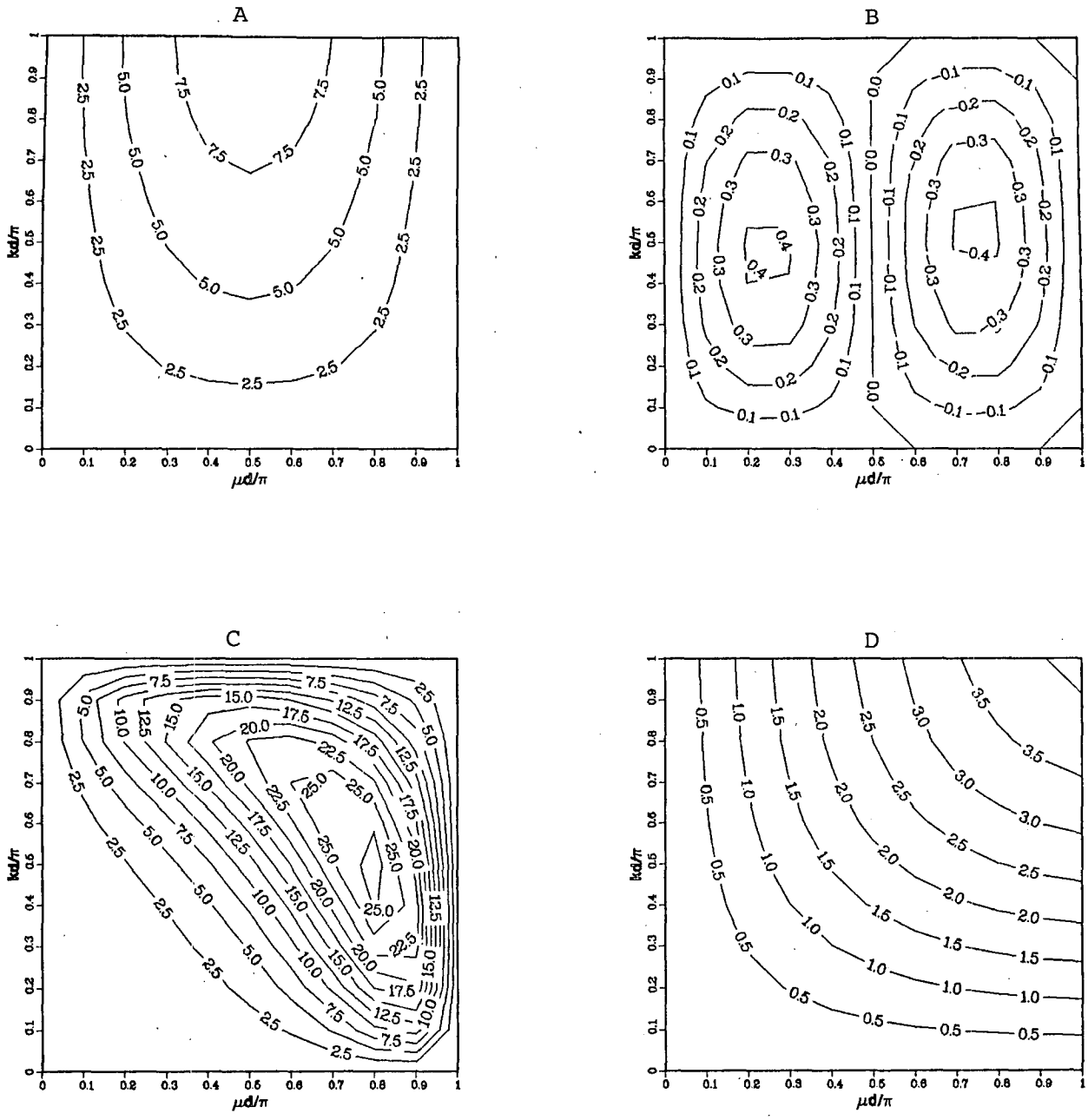

FIG. 8: Same as Fig. 5 except that $r^2 = 10$.

size is smaller than, the same order as, or larger than the Rossby radius of deformation. The Rossby radius of deformation can be written in terms of the equivalent depth so that various vertical modes can be considered.

The results show that all schemes converge in the large scale limit ($\mu d, kd \rightarrow 0$). For the case where the grid size is smaller than the Rossby radius of deformation [$d^2/(4\lambda^2) = 0.1$] grid C is the best of the primitive equation schemes because grids A and B both give spuriously large group velocities when the wave resolution is poor. All of the vorticity-divergence schemes give good results, with the isosceles triangle FEM being the best. The arrangement of model points in the isosceles triangle FEM is favorable for evaluation of the beta term in the vorticity equation, and this effect for advection has also been discussed by Neta and Williams (1986). When the grid size is of the order of the Rossby radius [$d^2/(4\lambda^2) = 1.0$], all the numerical schemes

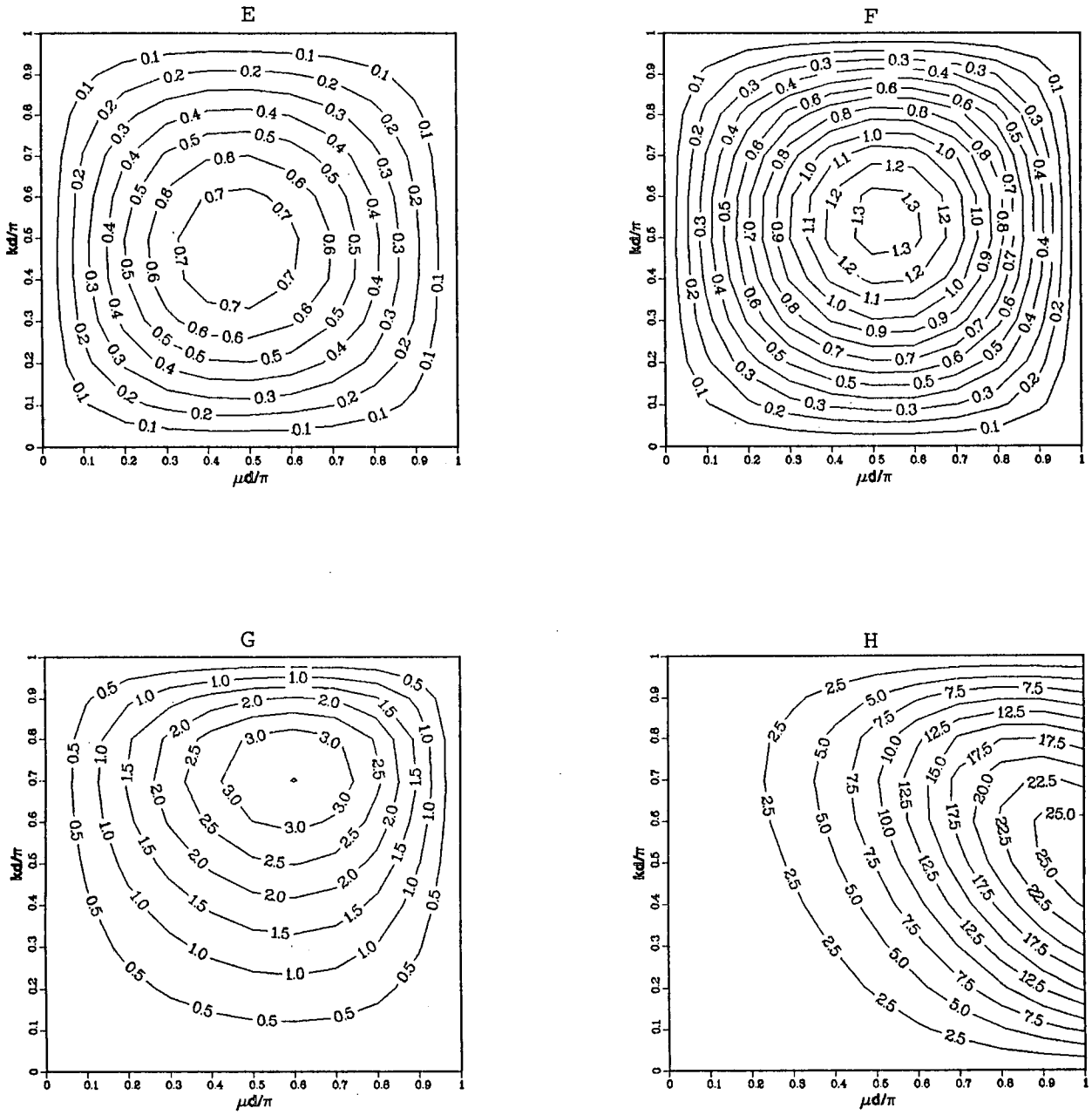

FIG. 8. (*Continued*)

have a reasonable behavior with the isosceles triangle and the rectangle finite element schemes giving the best results. For the case where the grid size is greater than the Rossby radius [$d^2/(4\lambda^2) = 10$] primitive equation grid C has very large group velocities when the wave resolution is poor. The rectangular finite element scheme gives the best solution.

Wajsowicz (1986) pointed out the large group velocities for the grid C finite difference could lead to serious errors in western boundary current simulations in baroclinic ocean models and that scheme B could also have problems. In addition we have found that finite difference scheme A can also be poor on the boundaries.

Our results show that numerical schemes based on the vorticity-divergence form of the shallow water equations give better Rossby wave simulations on the whole than schemes based on the primitive form of

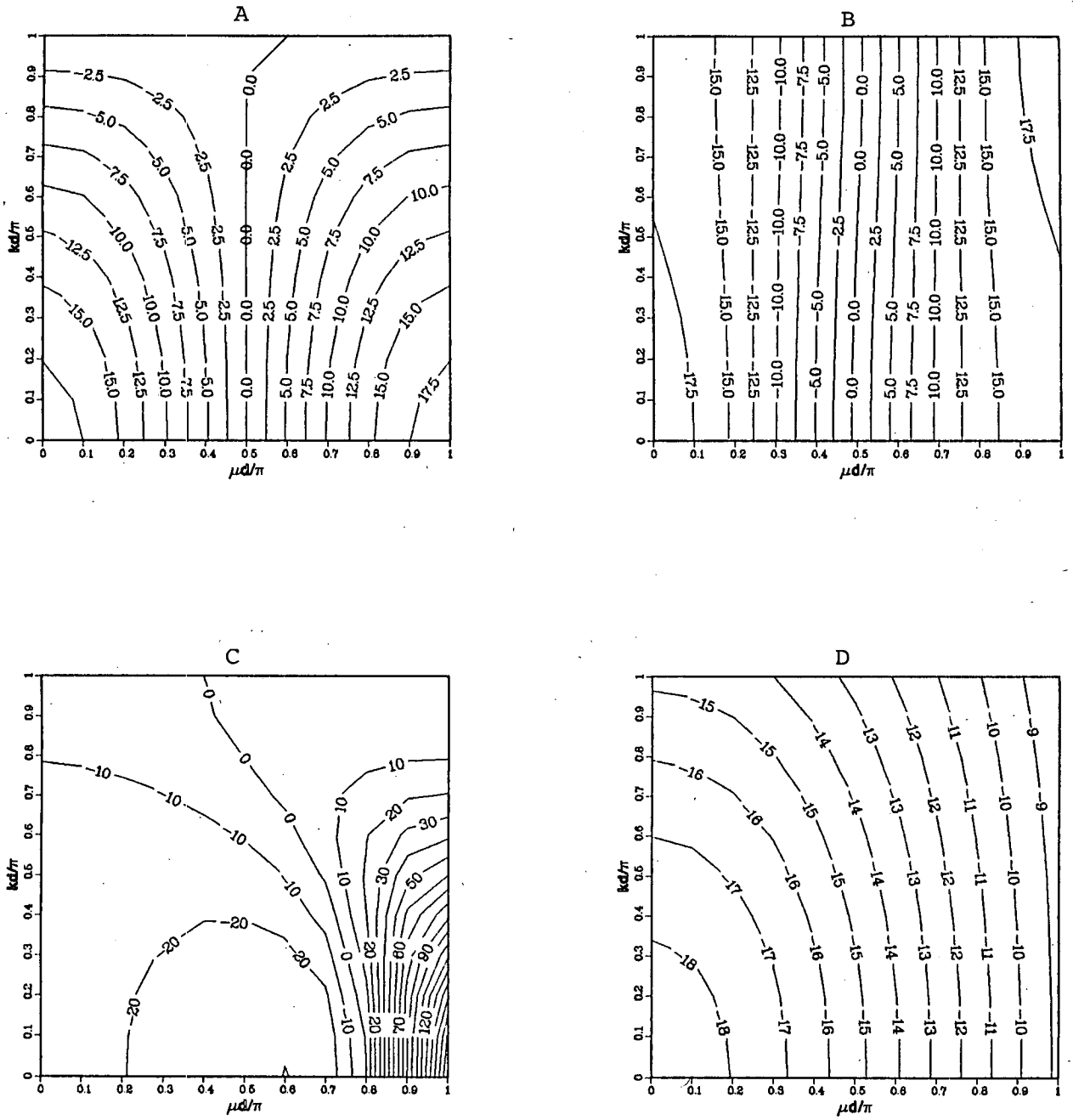

FIG. 9. Same as Fig. 6 except that $r^2 = 10$.

the shallow water equations. This is not surprising because Rossby wave dynamics are partially or totally controlled by the vorticity equation, and the discrete vorticity equation derived from the discrete equations of motion will normally have more truncation error.

These results indicate that a finite element vorticity-divergence model would be particularly useful for ocean prediction since these models have excellent advective and geostrophic adjustment properties (see Neta and Williams 1986 and Williams 1981), and they can be used easily with variable element size. Staniforth and Daley (1979) and Cullen and Hall (1979) have demonstrated the effectiveness of this type of model for atmospheric prediction.

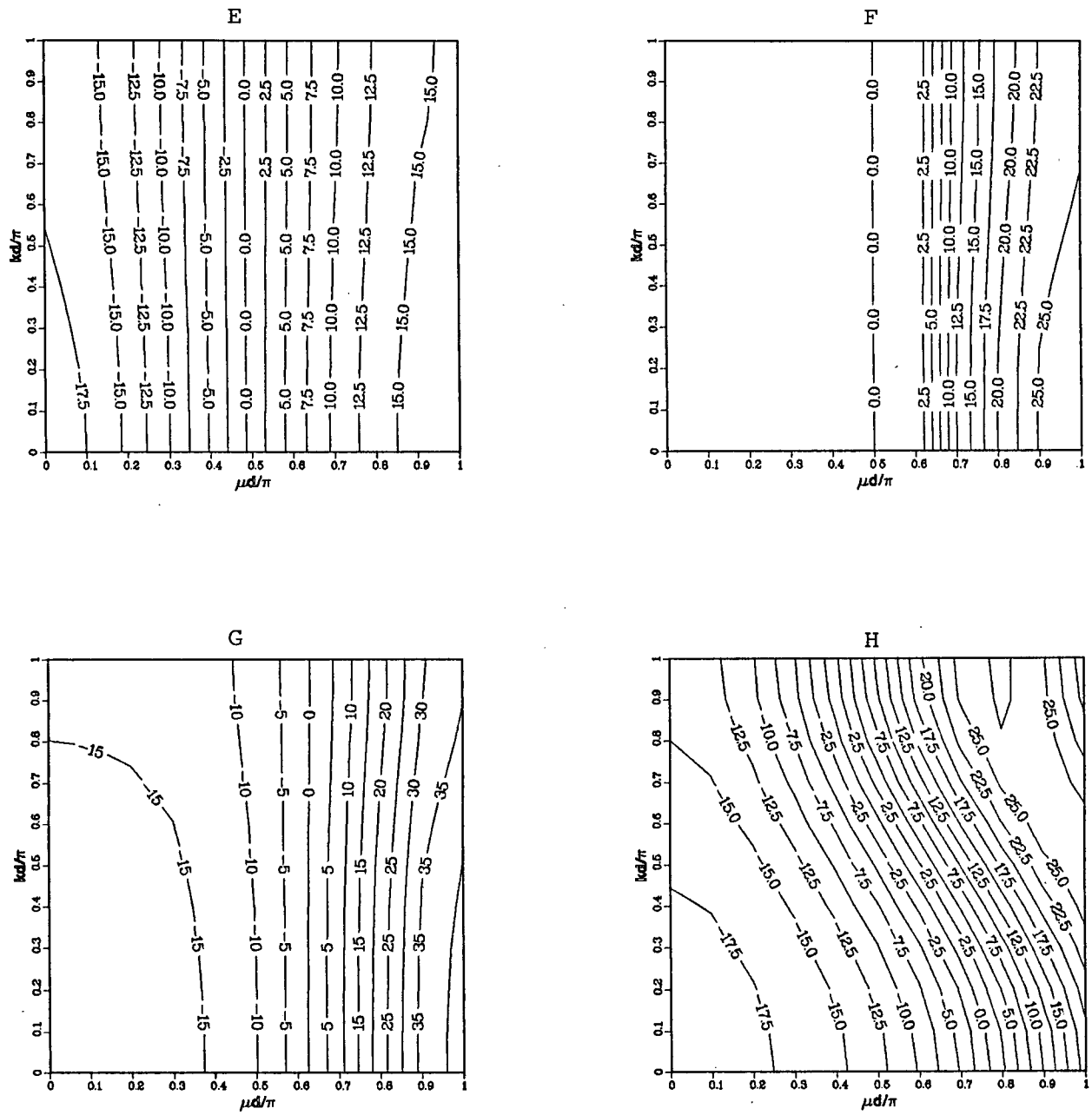

FIG. 9. (*Continued*)

Acknowledgments. The authors would like to thank Dr. A. N. Staniforth for his careful review of the manuscript. This research was conducted for the Office of Naval Research and was funded by the Naval Postgraduate School. The manuscript was carefully typed by Ms. P. Jones and Ms. J. Murray, and the numerical calculations were carried out at the W. R. Church Computer Center.

APPENDIX A

Coefficients for Finite Element Schemes

We illustrate the general procedure by deriving (3.1) from (2.7). First express the dependent variables in terms of the basis functions $\phi_i(x, y)$ as follows:

$$\begin{bmatrix} \zeta \\ D \\ h \end{bmatrix} = \sum_j \begin{bmatrix} \zeta_j \\ D_j \\ h_j \end{bmatrix} \phi_j. \quad \text{(A.1)}$$

To apply the Galerkin procedure we substitute (A.1) into (2.7), multiply by ϕ_i and integrate over the domain to force the error to be orthogonal to the basis functions giving

$$\sum_j \dot{\zeta}_j \int_T \phi_i \phi_j dA + f_0 \sum_j D_j \int \phi_i \phi_j dA + \frac{\beta_0}{f_0} \sum_j h_j \int_T \phi_i \frac{\partial \phi_j}{\partial x} dA = 0. \quad \text{(A.2)}$$

The isosceles triangle basis function is shown in Fig. A1. The following expressions for integration over the triangles can be found in Zienkiewicz (1977):

$$\int_T \phi_i \phi_j dA = \begin{cases} A/6 & i = j \\ A/12 & i \neq j, \end{cases} \quad \text{(A.3)}$$

$$\int_T \phi_i \frac{\partial \phi_j}{\partial x} dA = b_j/6, \quad \text{(A.4)}$$

$$\int_T \phi_i \frac{\partial \phi_j}{\partial y} dA = a_j/6, \quad \text{(A.5)}$$

$$\int_T \frac{\partial \phi_j}{\partial x} \frac{\partial \phi_i}{\partial x} dA = \frac{b_i b_j}{4A}, \quad \text{(A.6)}$$

$$\int_T \frac{\partial \phi_i}{\partial y} \frac{\partial \phi_j}{\partial y} dA = \frac{a_i a_j}{4A}, \quad \text{(A.7)}$$

where T is a triangular element, A is the area of T and a_j and b_j are defined by

$$a_1 = x_3 - x_2, \quad b_1 = y_2 - y_3,$$
$$a_2 = x_1 - x_3, \quad b_2 = y_3 - y_1,$$
$$a_3 = x_2 - x_1, \quad b_3 = y_1 - y_2.$$

The vertices of the triangle (x_j, y_j) are numbered counterclockwise. When (A.2) is evaluated for the isosceles triangles we obtain

$$\dot{\zeta}_{0,0} + \frac{1}{6}[\dot{\zeta}_{1,0} + \dot{\zeta}_{-1,0} + \dot{\zeta}_{1/2,1} + \dot{\zeta}_{-1/2,1} + \dot{\zeta}_{1/2,-1} + \dot{\zeta}_{-1/2,-1}] + f_0 \left\{ D_{0,0} + \frac{1}{2}[D_{1,0} + D_{-1,0} + D_{1/2,1} + D_{-1/2,1} + D_{1/2,-1} + D_{-1/2,-1}] \right\} + \frac{\beta_0}{3 f_0 \Delta x}\{2[h_{1,0} - h_{-1,0}] + h_{1/2,1} + h_{-1/2,1} + h_{1/2,-1} + h_{-1/2,-1}\} = 0, \quad \text{(A.8)}$$

where each triangle has a base of Δx and a height of Δy. The super dot indicates a partial time derivative and $D_{1/2,-1}$ is equal to $D(x + \Delta x/2, y - \Delta y)$. The final form of (3.1) is obtained by introducing the spatial dependence $\exp[i(\mu x + ky)]$ for each dependent variable. Equations (3.2) and (3.3) are obtained in the same manner but integration by parts is required for the Laplacian of h in (2.8).

The equations for the bilinear basis functions on rectangles are obtained in the same manner as with the triangles. The integration formulae corresponding to (A.3) to (A.7) are given by Staniforth and Mitchell (1977), and the details will not be reproduced here.

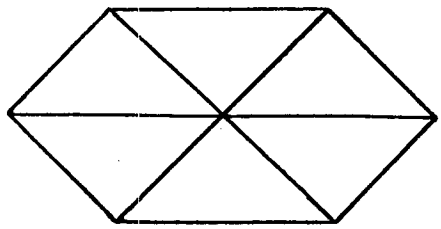

FIG. A1. The isosceles triangle basis function.

APPENDIX B

Coefficients for Finite Difference Scheme A

The coefficients for the nonstaggered finite difference scheme A are derived here. The equation set (2.1)–(2.3) for this scheme can be written

$$\frac{\partial u}{\partial t} - fv + g\overline{\delta_x h}^x = 0, \quad \text{(B.1)}$$

$$\frac{\partial v}{\partial t} + fu + g\overline{\delta_y h}^y = 0, \quad \text{(B.2)}$$

$$\frac{\partial h}{\partial t} + H(\overline{\delta_x u}^x + \overline{\delta_y v}^y) = 0, \quad \text{(B.3)}$$

where, for example,

$$\delta_x h = [h(x + \Delta x/2) - h(x - \Delta x/2)]/\Delta x$$

and

$$\bar{h}^x = [h(x + \Delta x/2) + h(x - \Delta x/2)]/2.$$

To obtain the vorticity-divergence formulation we let

$$\zeta = \overline{\delta_x v}^x - \overline{\delta_y u}^y,$$
$$D = \overline{\delta_x u}^x + \overline{\delta_y v}^y. \quad \text{(B.4)}$$

By subtracting and adding (B.1) and (B.2) and using (B.4) the vorticity-divergence system becomes

$$\frac{\partial \zeta}{\partial t} + fD + \beta \bar{v}^{2y} = 0, \quad \text{(B.5)}$$

$$\frac{\partial D}{\partial t} - f\zeta - \beta\bar{u}^{y} + g(\overline{\delta_x^2 u}^{xx} + \overline{\delta_y^2 v}^{yy}) = 0, \quad \text{(B.6)}$$

$$\frac{\partial h}{\partial t} + HD = 0, \quad \text{(B.7)}$$

where $f = f_0 + \beta y$ and $\bar{v}^{2y} = [v(y + \Delta y) + v(y - \Delta y)]/2$ is used to develop this form. The quasi-geostrophic set is obtained by replacing (B.5) and (B.6) with

$$\frac{\partial \zeta}{\partial t} + f_0 D + \frac{\beta}{f_0} g\delta_x \overline{\bar{h}^{x}}^{2y} = 0, \quad \text{(B.8)}$$

$$-f_0\zeta + g(\overline{\delta_x^2 h}^{xx} + \overline{\delta_y^2 h}^{yy}) = 0, \quad \text{(B.9)}$$

which are analogous to (2.7) and (2.8). The required coefficients can be obtained by substituting the wave forms into (B.7), (B.8), and (B.9).

REFERENCES

Arakawa, A., and V. R. Lamb, 1977: Computational design of the basic dynamical processes of the UCLA general circulation model. *Methods in Computational Physics,* Vol. 17, Academic Press, 173–265.

Cote, J., M. Beland and A. Staniforth, 1983: Stability of vertical discretization schemes for semi-implicit primitive equation models: theory and applications. *Mon. Wea. Rev.,* **111,** 1189–1207.

Cullen, M. J. P., and C. D. Hall, 1979: Forecasting and general circulation results from finite element models. *Quart. J. Roy. Meteor. Soc.,* **105,** 571–592.

Gill, A. E., 1982: *Atmosphere-Ocean Dynamics.* Academic Press, 622 pp.

Haltiner, G. J., and R. T. Williams, 1980: *Numerical Weather Prediction and Dynamic Meteorology.* Wiley, 477 pp.

Mesinger, F., 1979: Dependence of vorticity analogue and the Rossby wave phase speed on the choice of horizontal grid. *Sciences Mathematiques,* **10,** 5–15.

Neta, B., and R. T. Williams, 1986: Stability and phase speed for various finite element formulations of the advection equation. *Comput. Fluids,* **14,** 393–410.

——, —— and D. E. Hinsman, 1986: Studies in a shallow water fluid model with topography. *Numerical Mathematics and Applications,* R. Vichnevetsky and J. Vignes, Eds., Elsevier, 347–354.

Schoenstadt, A. L., 1980: A transfer function analysis of numerical schemes used to simulate geostrophic adjustment. *Mon. Wea. Rev.,* **108,** 1248–1259.

Staniforth, A. N., and H. L. Mitchell, 1977: A semi-implicit finite-element barotropic model. *Mon. Wea. Rev.,* **105,** 154–169.

——, and ——, 1978: A variable resolution finite-element technique for regional forecasting with the primitive equations. *Mon. Wea. Rev.,* **106,** 439–447.

——, and R. W. Daley, 1979: A baroclinic finite-element model for regional forecasting with the primitive equations. *Mon. Wea. Rev.,* **107,** 107–121.

Wajsowicz, R. C., 1986: Free planetary waves in finite-difference numerical models. *J. Phys. Oceanogr.,* **16,** 773–789.

Williams, R. T., 1981: On the formulation of finite-element prediction models. *Mon. Wea. Rev.,* **109,** 463–466.

Zienkiewicz, O. C., 1977: *The Finite Element Method in Engineering Science.* Wiley, 787 pp.